

# Methods for Real-Time Rotor Stall Detection

Ivan Grill

*Graduate Research Assistant  
School of Aerospace Engineering  
Georgia Institute of Technology  
Atlanta, GA 30332*

Manuj Dhingra

*Research Engineer  
School of Aerospace Engineering  
Georgia Institute of Technology  
Atlanta, GA 30332*

J.V.R. Prasad

*Professor  
School of Aerospace Engineering  
Georgia Institute of Technology  
Atlanta, GA 30332*

## Abstract

Main rotor stall in rotorcraft is characterized by the loss of lift, increased vibrations and significant structural loads on the rotor control system. The main focus of the current study is to examine an effective method for real time detection of rotor stall. The discussion related to rotor stall specifically pertains to an increase in control system pitch link loads. Observations related to various aerodynamic phenomena that influence the pitch link loads are discussed as well. Data from the UH-60A Airloads Project obtained through the TRENDS database are used in this study. An existing method based on the Equivalent Retreating Indicated Tip Speed (ERITS) measure is evaluated using the UH-60A data, and is shown to be overly conservative for rotor stall detection, both during steady and maneuvering flight conditions. A new method based on a previously developed Real-Time Nonlinear Observer algorithm is evaluated for its applicability to real time rotor stall detection and is shown to be a viable alternative.

## Nomenclature

$c$	blade chord
$C_L$	blade lift coefficient
$C_W$	aircraft weight coefficient
$D$	total aircraft drag
$h$	altitude
$L$	blade lift
$N_b$	number of rotor blades
$N_z$	load factor along the body z-axis
$R$	blade radius
$S$	blade surface area
$T$	main rotor thrust
$V$	aircraft true airspeed
$V_i$	aircraft indicated airspeed
$V_{rel}$	blade relative airspeed
$W$	aircraft current weight
$W_0$	aircraft nominal weight (arbitrary) = 73396 N
$\rho$	air density
$\rho_{SL}$	sea level standard air density
$\sigma$	main rotor solidity ( $N_b c / \pi R$ )
$\omega$	pitch link load frequency
$\Omega$	main rotor angular velocity

## Introduction

Main rotor stall is one of the major factors that limit the high speed forward flight and impact the maneuverability of a rotorcraft. The vibrations produced by a stalling rotor may significantly damage the rotorcraft's control system. This structural damage typically requires costly and time consuming repairs but in extreme cases can impede

pilot's ability to maneuver the aircraft. The term "rotor stall" is used in the current study to designate the rotorcraft flight condition in which a significant portion of the rotor disc has stalled, such that the rotor control loads have increased beyond a prescribed limit. Further, the term "control loads" refers specifically to the loads on the main rotor pitch links which, as the name suggests, are responsible for the blade pitch control. The main rotor control system contains pitch links in both the fixed as well as in the rotating frame. It will be shown that the effects of rotor stall are different for the fixed and rotating pitch links, and hence it is important to distinguish them clearly. A detailed description of a generic main rotor control system along with an accompanying schematic is available in Ref. [1]. It is also important to distinguish between rotor stall and blade stall, because the presence of stall at a few sections only of a rotor blade does not necessarily imply significant increase in pitch link loads. However, in order to understand rotor stall, we need to understand the individual blade stall as well. The mechanisms responsible for rotor blade dynamic stall and its effects are presented in significant detail by McCroskey [2] and Young [3]. In forward flight, rotor blade experiences airflow from vehicle motion as well as its own rotation. The effective flow becomes asymmetric, with higher velocities on the advancing side and lower velocities on the retreating side of the rotor disc. In order to compensate for the lower relative velocity on the retreating side, the blade goes through a cyclic pitch (feathering) motion. That means that the blade pitch and therefore blade angle of attack must be higher on the retreating side. If the angle of attack is too high, the blade will exhibit dynamic stall. As the blade stalls, the top

surface pressure in the front part of the blade increases due to loss of suction. This, in turn causes the center of pressure to move towards the trailing edge, creating a short-term but large magnitude negative pitching moment, which is the root cause of oscillating pitch link loads as the rotor enters stall. Although computational techniques have been used to understand and predict the effect of dynamic stall on pitch link loads, e.g. Datta and Chopra [4], a real-time oriented model has not been developed so far.

An overview of various approaches to the problem of rotor stall is presented in the following paragraph. Since rotor stall is a consequence of blade stall occurring over a significant portion of a rotor disc, one way of avoiding rotor stall is to prevent blade stall itself. Considerable amount of research has been done related to the retreating blade stall control and some of it is presented by Nguyen [5] and Lorber et al. [6]. Blade stall control requires that the blade be instrumented with actuators in case of an open loop control, and with sensors and actuators in case of a closed loop control. Additional instrumentation however brings up an issue of complexity associated with blade stall control system integration, which is quite significant [6]. In addition to the individual blade stall control, some work has also been done in the area of pitch link loads reduction using control techniques by Voskuijl et al. [7]. Unfortunately, due to the lack of experimental data available to Voskuijl and others, no clear conclusions were made about the obtained results. In the absence of physics based models, neural networks could be applied for pitch link load prediction, if the experimental data required for training of the neural network was available. Kottapalli [8] has shown that the neural network approach can accurately model the pitch link loads in level flights and maneuvers. However, the neural network approach suffers from the disadvantage that it requires large amounts of training and validation data covering the entire range of flight conditions.

Current methods utilized for rotor stall detection use empirical parameters obtained from numerous flight tests and experience in order to set a limit on the aircraft's flight envelope. One of the empirical parameters that set the limit on the rotorcraft airspeed for an allowable level of control loads is shown in Ref. [1] and is represented by  $k$ . Expression for the aircraft velocity limit as a function of  $k$  is shown in Equation 1.

$$V_{\text{lim}} \approx \Omega R - \sqrt{\frac{k}{\rho W}} \quad (1)$$

No detailed explanation of the origin of  $k$  is given, except for the fact that it is a function of both blade geometry and loading. However, another parameter directly analogous to  $k$  is Equivalent Retreating Indicated Tip Speed (ERITS), which is proportional to  $1/\sqrt{C_L}$ , where  $C_L$  is the equivalent lift coefficient of the retreating blade near the tip at 270° azimuth with a simplifying assumption of uniform lift distribution. ERITS itself is not obtained empirically but the limit that needs to be set on ERITS is an empirical value. Therefore ERITS itself will be considered an empirical rotor stall detection parameter. There does not seem to be any written references related to the origins of ERITS, for it is a parameter that was originally developed at Sikorsky as an “in-house” rotor stall detection method. Some studies have considered ERITS as a viable rotor stall detection method, particularly the works of Jeram [9] and Yavrucuk et al. [10]. Considering that ERITS is the only method specifically formulated as a rotor stall detection parameter, its applications and derivation will be discussed in further detail.

The current study has a dual focus: a deeper understanding of the fundamental aerodynamic phenomena that affect the pitch link loads as well as a feasibility investigation of real-time rotor stall detection. The analysis of the ERITS parameter presented here illustrates its limitations as a rotor stall detection method. Consequently, a new method for rotor stall detection that utilizes the fixed frame pitch link load measurements has been proposed and evaluated using flight test data. The proposed method tracks the frequency content of the pitch link load signal using a real-time algorithm previously developed at the Georgia Institute of Technology. This signal processing algorithm, called the Real-Time Nonlinear Observer (RTNO), has the ability to extract the magnitude and frequency of the dominant component in a signal. Data used throughout this study are obtained through the TRENDS database [11], which contains flight test data generated as part of the UH-60A Airloads Project.

The paper presented is organized as follows: First, a brief description of the database which is the source of all the data used in the current study is presented. Next, the various aerodynamic phenomena that influence the pitch link loads are discussed, in order to gain a better understanding of the problem at hand. This is followed by the discussion of the evaluation of the ERITS method and the proposed RTNO method for real time stall detection. Finally, concluding remarks are provided in order to summarize the main points of the study along with suggestions for future work.

## UH-60A Airloads Data

Data used in the current study are obtained from the TRENDS database, which consists of numerous flight test data generated in 1993-1994, as part of the UH-60A Airloads Project at NASA Ames Research Center [12]. The test aircraft was a four bladed utility helicopter UH-60A Blackhawk, with two fully instrumented blades. One blade was instrumented with 242 pressure transducers and another with various strain gauges and accelerometers. In addition to the blades, strain gauges were also placed on each fixed and rotating pitch link, and accelerometers were installed at various stations on the fuselage. The term “counter” used in the following discussion refers to the set of data measured during a specific flight at some particular flight condition. In other words, during each test flight, multiple counters were recorded by the flight crew, each at a specific flight condition. Counters are designated by a four or five digit number where the first two out of four or three out of five digits refer to the flight number. For example, counter 9017 was recorded during the flight 90 and counter 11023 during flight 110. List of counters considered in this paper along with some of their flight parameters are shown in Table 1. These counters represent only a fraction of the total test data generated during the UH-60A Airloads Project. More detailed information referring to the TRENDS database is provided by Bondi and Bjorkman [11] while the details of the UH-60A Airloads Project may be found in [12].

**Table 1: Flight Parameters for Various Counters**

Counter	$V_i$ [m/sec]	$C_W/\sigma$	$N_z$	h [m]	Flight Condition
8919	51.96	0.11	1.0	3658	Level Flight
9011	34.98	0.13	1.0	5182	Level Flight
9012	32.92	0.13	1.0	5182	Level Flight
9013	26.75	0.13	1.0	5182	Level Flight
9017	35.50	0.13	1.0	5182	Level Flight
11022	61.73	0.08	1.85	1676	Pull-Up
11023	61.73	0.08	2.25	1676	Pull-Up

### Effects of Rotor Stall on Pitch Link Loads

Performance of a rotorcraft is limited by multiple phenomena which depend on the flight condition. According to Coleman and Bousman [13], limiting performance at low to moderate weight coefficients and high advance ratios is caused by increased drag near the blade tip on the advancing side of the blade. This drag is due to the development of the supercritical flow and moderate to strong shockwaves on both the top and bottom surfaces of the blade, and has nothing to do with the blade stall. On the other

hand, performance at high weight coefficients is limited by the dynamic stall cycles which seem to be the main cause of the increased pitch link loads. Coleman and Bousman [13] claim that the increase in pitching moments at high advance ratios is caused by unsteady, three dimensional flow at the blade tip which is unrelated to stall. However, it will be shown using the flight test data that high advance ratio does not necessarily correspond to significant increase in pitch link loads if the weight coefficient is low. At high advance ratio, the increase in drag on the advancing blade does not limit the aircraft performance by increasing the structural loads, but by increasing the required power. Counters 9017 and 8919 shown in Table 1 correspond to two flight conditions with significantly different pitch link loads, but nearly identical required power (within 3%), where counter 9017 corresponds to the most severe level flight condition with the highest pitch link loads. In fact, all level flights tested during the UH-60A Airloads Project had the same limiting condition, a 30-minute engine power limit according to Kufeld et al. [12], which refers to the maximum power that the engines are allowed to generate continuously for no more than 30 minutes. So even though both of these flights were limited by power requirement, one flight experienced significant level of rotor stall while the other did not. This implies that what ever phenomena occurs on the advancing blade at high advance ratios, it is not nearly as significant to the increase in pitch link loads as the retreating blade stall at high weight coefficients. Therefore, if the aircraft is flying at the flight condition where its performance is limited by factors other than the retreating blade stall, the level of pitch link loads will not deviate significantly from the nominal range.

It is expected that the retreating blade stall should occur near 270° azimuth position. Stall will not occur exactly at 270° azimuth position, because the blade will have a maximum pitch slightly beyond 270° azimuth, due to the lateral thrust contribution needed to counter the tail rotor thrust. Azimuth orientation for counterclockwise rotation is shown in Figure 1. The retreating blade does not necessarily always stall only at 270° azimuth position. This can be observed in Figure 1 [14], which shows the radial and azimuth locations of the blade stall identified by the abrupt reduction in sectional pitching moments. According to Bousman [14], first occurrence of stall between 230° and 290° azimuth is due to the high angles of attack. The pitching moment due to this initial stall leads to blade torsional oscillations that in turn lead to the subsequent stall region observed near the 340° azimuth. Therefore the second stall is primarily a function of the blade torsional stiffness and the

rotating pitch link stiffness. The effects of rotor control system stiffness on the blade response during the dynamic stall have been examined by Kufeld and Johnson [15].

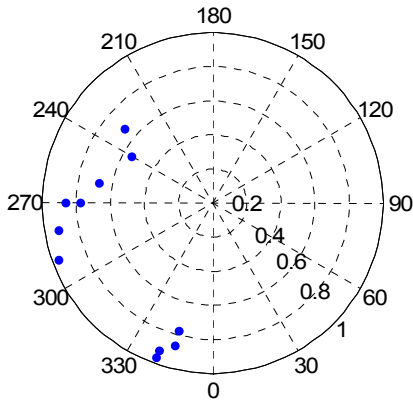


**Figure 1: Dynamic Stall Locations for Counter 9017**

Another interesting phenomenon associated with the pitch link loads is the fact that, even the cases with relatively low pitch link loads, compared to counter 9017, exhibit blade stall. For example, counter 9013 shows a region of significant stall near 270° azimuth at 0.865R radial location and a minor stall region near 350° azimuth. Counters 9011, 9012 and 9017 all show significant stall at both 270° and 350° azimuth locations. Figure 2 shows these stall regions at 0.865R for all four mentioned level flights. If this type of stall occurs at large enough number of radial locations, then the large negative blade pitching moment will develop. These negative pitching moments are then transferred to the rotating pitch links. Figure 2 and Figure 3 illustrate how an abrupt drop in sectional pitching moments is transferred to the rotating pitch links, such that the rotating pitch link loads themselves exhibit an abrupt drop near the same azimuth location. Loads shown in Figure 3 and Figure 4 illustrate how rotating pitch link loads affect fixed pitch link loads as the rotor approaches stall. These affects may be clarified with Figure 5 and Figure 6 which show spectral analysis results obtained from the data shown in Figure 3 and Figure 4 for rotating and fixed pitch link loads, respectively. From the time domain data shown in Figure 3 as well as from the frequency domain data shown in Figure 5, it is clear that the dominant load magnitude at 1/rev for rotating pitch links does not change significantly for level flights. Higher frequency content however clearly increases for rotating pitch links as rotor approaches stall as seen from the spectral analysis results in Figure 5. On the other hand, dominant magnitude at 4/rev for fixed

pitch links changes dramatically as shown in Figure 4 for the time domain and in Figure 6 for frequency domain. An explanation of these observations is as follows. Loads on the rotating pitch links are responsible for the forces and moments on the swash plate, which in turn cause the fixed pitch link loads. Forces on the swash plate result from the rotating pitch link loads at integer multiples of  $N_b/\text{rev}$ , and moments are due to the rotating pitch link loads at  $(nN_b \pm 1)/\text{rev}$ , where  $n$  is any positive integer [1]. Therefore the increase in rotating pitch link loads at 5/rev evident in Figure 5 could explain the increase in fixed pitch link loads at 4/rev in Figure 6. According to Ref. [1], these higher harmonic rotating pitch link load components are due to the blade torsional oscillations which are initiated by the first stall region near 270° azimuth as discussed earlier.

Same argument pertaining to Figure 2 through Figure 4 is also true for a pull-up maneuver results shown in Figure 7 through Figure 9. Data for only one pull-up maneuver are shown here since they represent the general trends observed for other pull-up maneuvers as well. Additional analysis of high load flights that include pull-ups as well as other maneuvers is presented by Kufeld and Bousman [16]. Figure 7 shows the sectional pitching moment at 0.865R for counter 11023 at four different rotor periods and Figure 8 shows the corresponding rotating pitch link loads. The relationship between sectional pitching moments in Figure 7 and rotating pitch link loads in Figure 8 is identical to the level flight case discussed earlier. Interesting observation in Figure 7 is the stall region near 50° azimuth for period 18 which is also shown by Bousman [14] for a pull-up maneuver. This stall region near 50° azimuth is a characteristic of maneuvers and does not appear during level flights. It is also observed that the sudden negative drop in sectional pitching moment near 50° azimuth location seen from Figure 7 does not affect rotating pitch link loads shown in Figure 8 for period 18. In fact, rotating pitch link loads show positive peak near 50° azimuth even though the sectional pitching moments exhibit negative peak at the same azimuth region. Figure 9 shows the fixed pitch link loads for the same rotor periods as Figure 7 and Figure 8. The loads shown in Figure 9 clearly indicate an abrupt increase in fixed pitch link loads during the 16<sup>th</sup> period. That is the period where the second stall region near 340° azimuth becomes significant, causing the increase in higher harmonic content of rotating pitch link loads. Increase in higher harmonic content is responsible for the increase in fixed pitch link loads as discussed earlier for level flights.

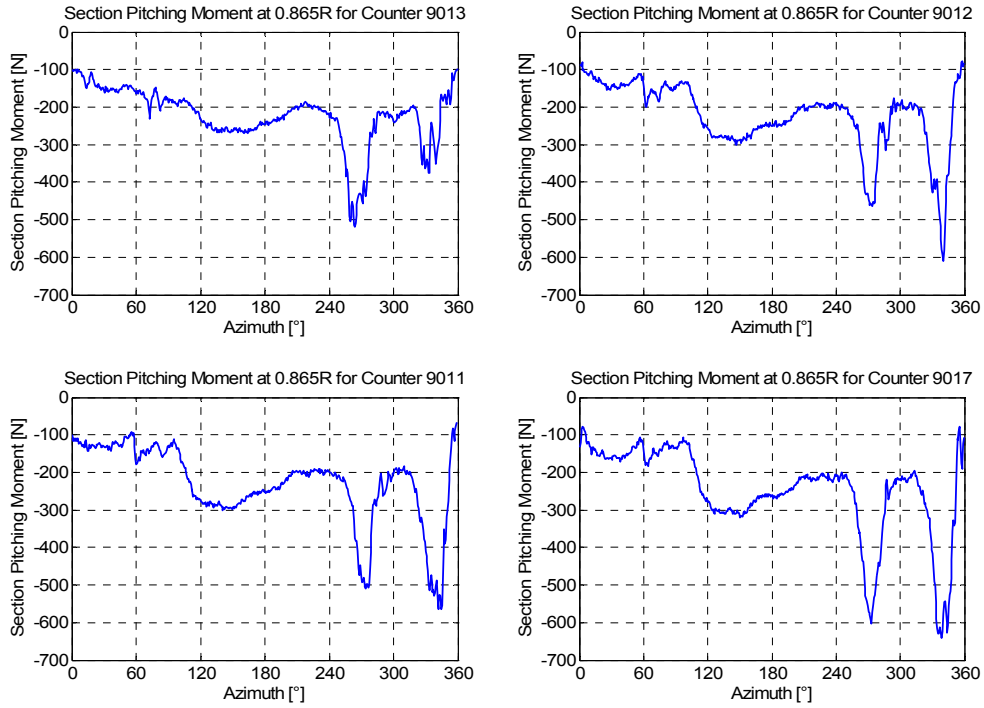


**Figure 2: Sectional Quarter Chord Pitching Moments for 4 Different Level Flights at 0.865R**

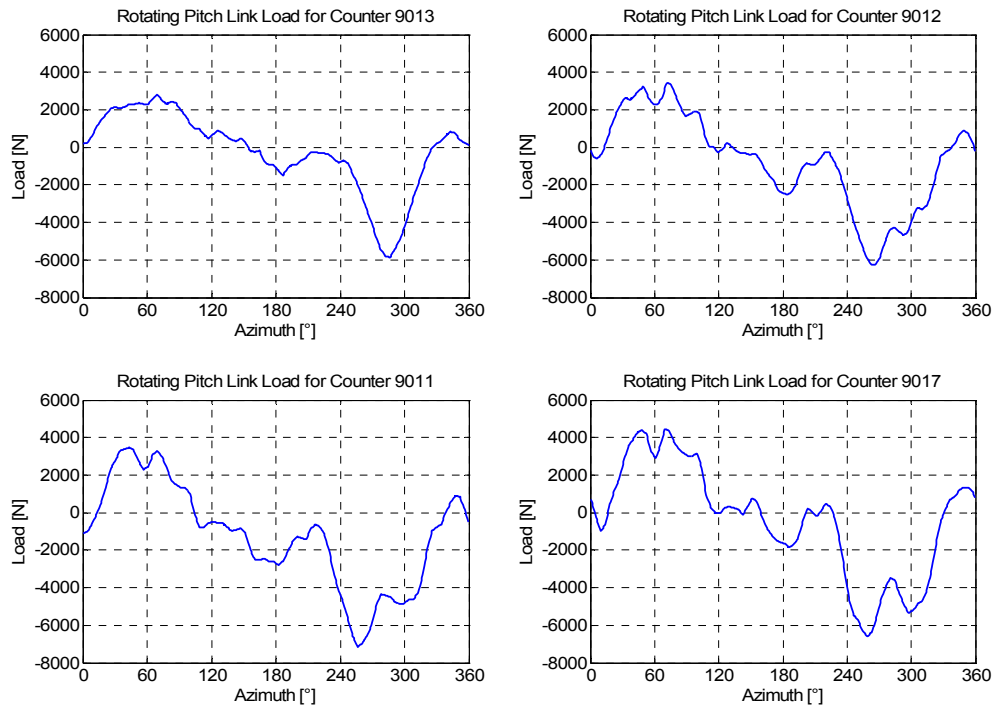


**Figure 3: Rotating Pitch Link #1 Loads for 4 Different Level Flights**

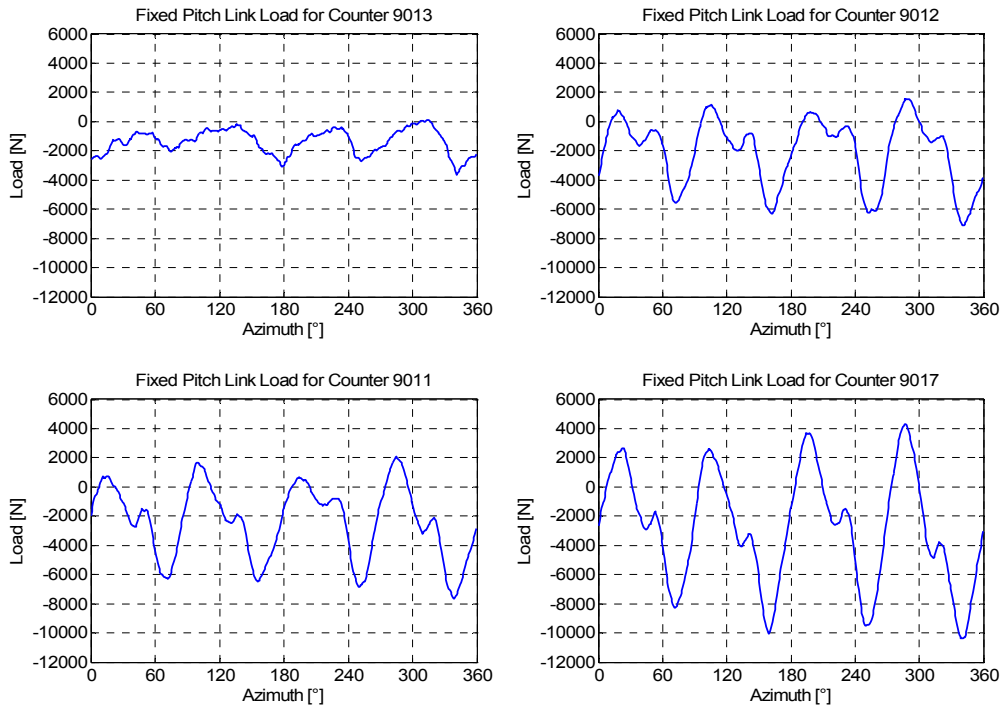


**Figure 4: Fixed Forward Pitch Link Loads for 4 Different Level Flights**

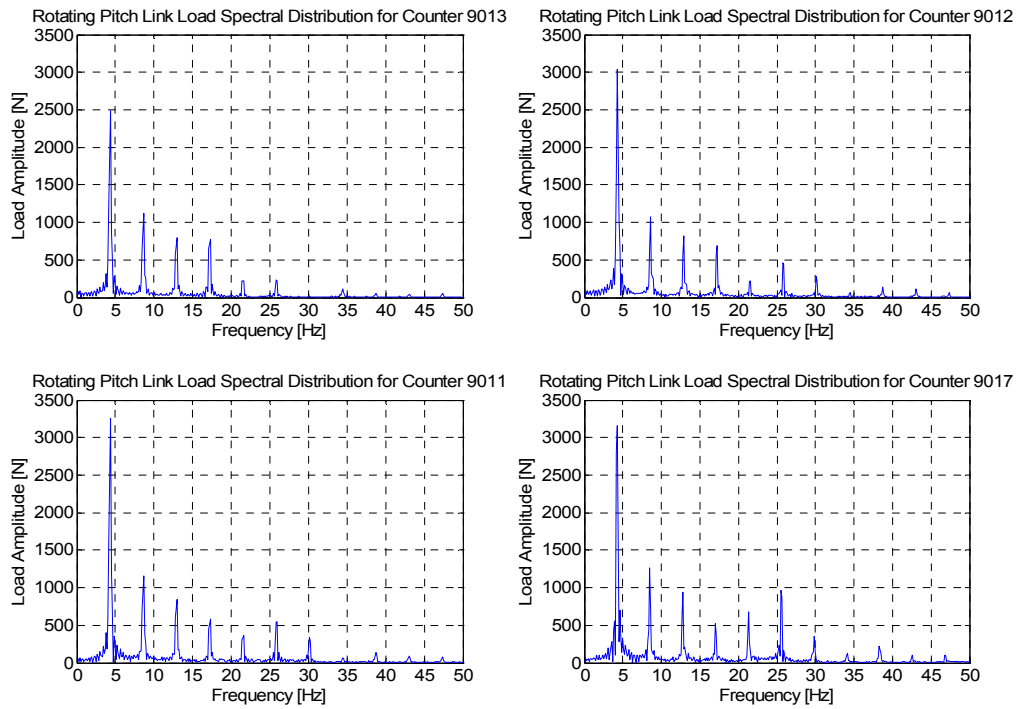


**Figure 5: Frequency Distribution of the Rotating Pitch Link #1 Loads for 4 Different Level Flights**

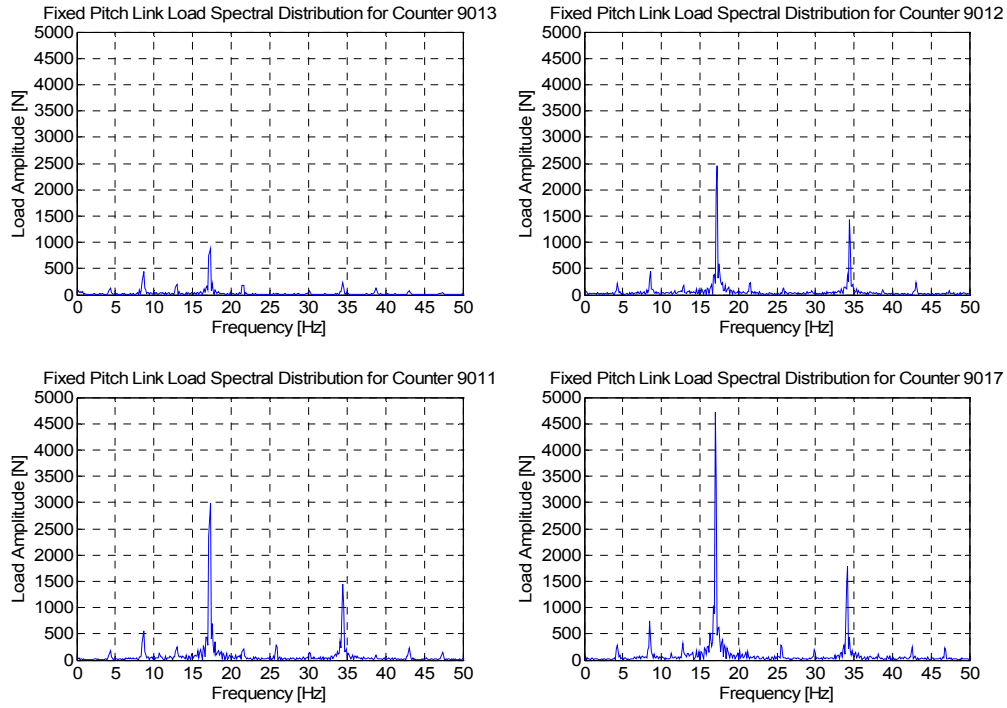


**Figure 6: Frequency Distribution of the Fixed Forward Pitch Link Loads for 4 Different Level Flights**

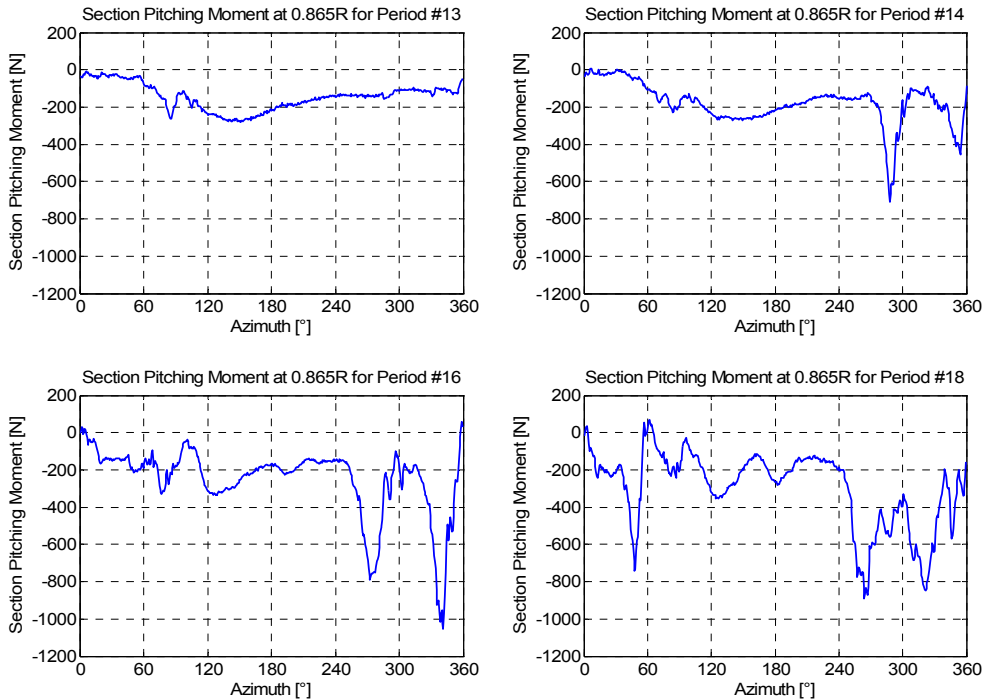


**Figure 7: Sectional Quarter Chord Pitching Moments for Pull-Up Maneuver at 0.865R For Counter 11023 (Periods 13, 14, 16 and 18)**

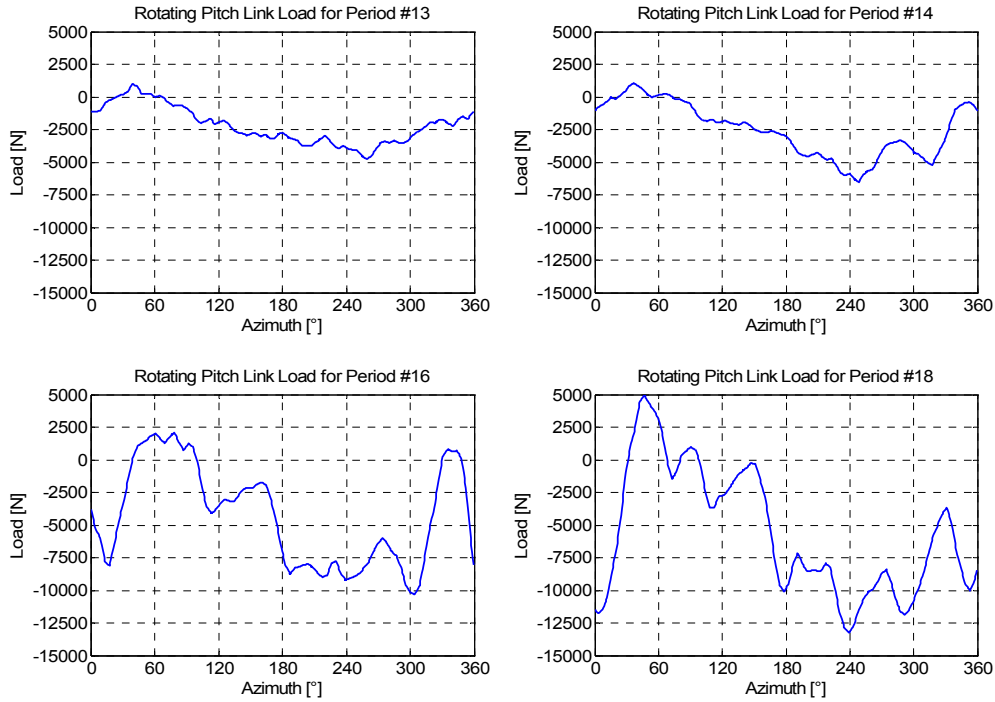


**Figure 8: Rotating Pitch Link #1 Loads for Pull-Up Maneuver For Counter 11023 (Periods 13, 14, 16 and 18)**

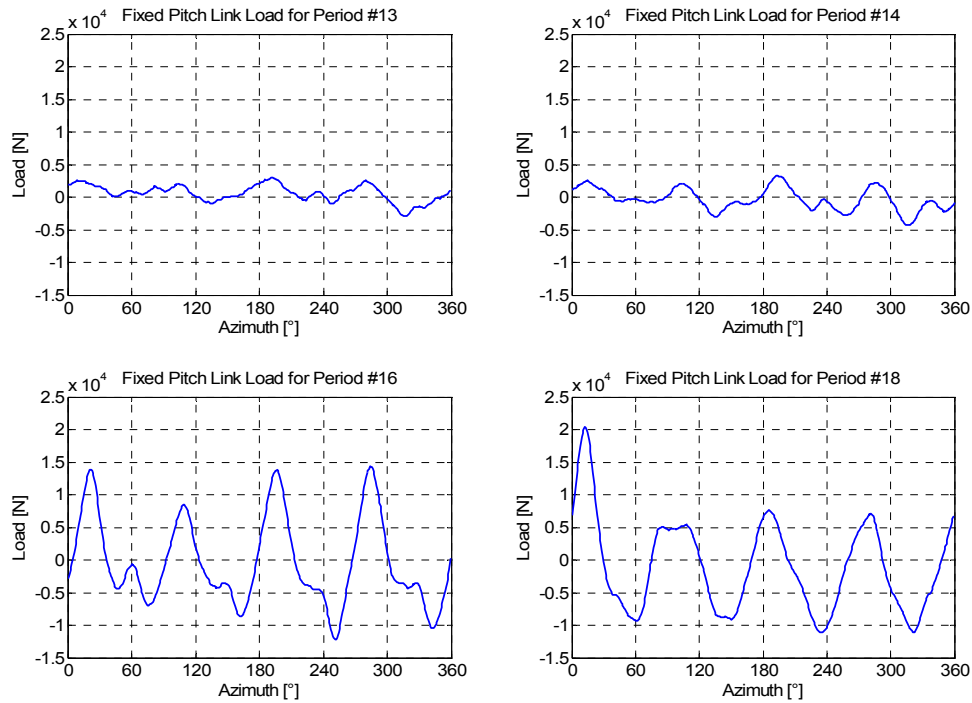


**Figure 9: Fixed Forward Pitch Link Loads for Pull-Up Maneuver For Counter 11023 (Periods 13, 14, 16 and 18)**

### Equivalent Retreating Indicated Tip Speed (ERITS)

One of the methods for the real-time rotor stall detection is an empirical parameter ERITS, originally developed at Sikorsky. ERITS is essentially a function of the retreating blade lift coefficient at 270° azimuth position. It is shown in the Appendix that ERITS is proportional to  $1/\sqrt{C_L}$ , where  $C_L$  is the equivalent lift coefficient of the retreating blade tip at 270° azimuth with an assumption that the lift distribution is uniform. Development of the ERITS expression is shown in the Appendix but the final expression is shown in Equation 2.

$$ERITS = \left( \Omega R \sqrt{\frac{\rho}{\rho_{SL}}} - V_i \right) \sqrt{\frac{W_0}{N_z W}} \quad (2)$$

It is found that low ERITS value does not always correspond to increased pitch link loads by studying the UH-60A pitch link load measurements. Some of these results are shown in Figure 10 and Figure 11 for a collection of level flights, and a few

representative maneuver flights, respectively. Each Figure shows the variation of the average fixed frame pitch link peak-to-peak loads vs. ERITS. Even though the fixed pitch link loads consist of more than just a 4/rev frequency content, dominant magnitude is at 4/rev. Therefore peak-to-peak values are determined at ¼ rotor revolution and are averaged over all periods for level flight data, and over each individual period for maneuvers. Therefore each point in Figure 10 corresponds to one level flight condition (one counter) while in Figure 11 each point corresponds to one rotor revolution for each maneuver flight condition.

Figure 10 shows that depending on the flight condition, low ERITS values will not always correspond to increased pitch link loads. Figure 11 shows that for low ERITS, the pitch link loads will increase only if the flight is maintained at that ERITS value. Therefore, only if the maneuver is sustained for some time will the loads increase. Also, same low ERITS values between maneuvers do not guarantee that the pitch link loads will be same either. This is why ERITS is not a robust measure of rotor stall.

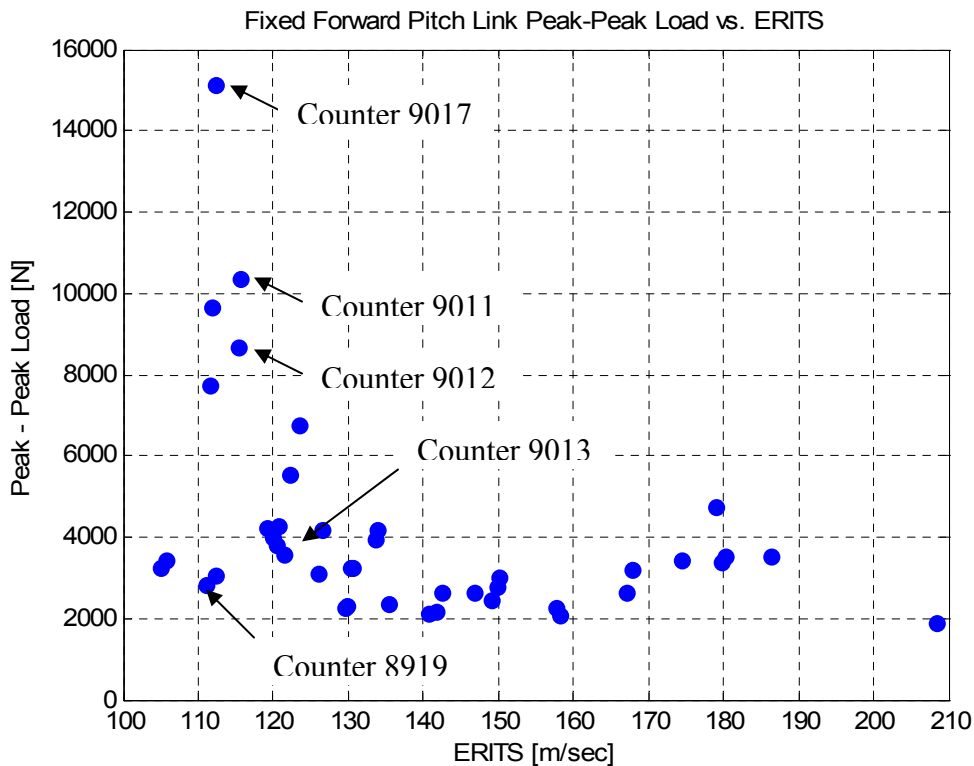
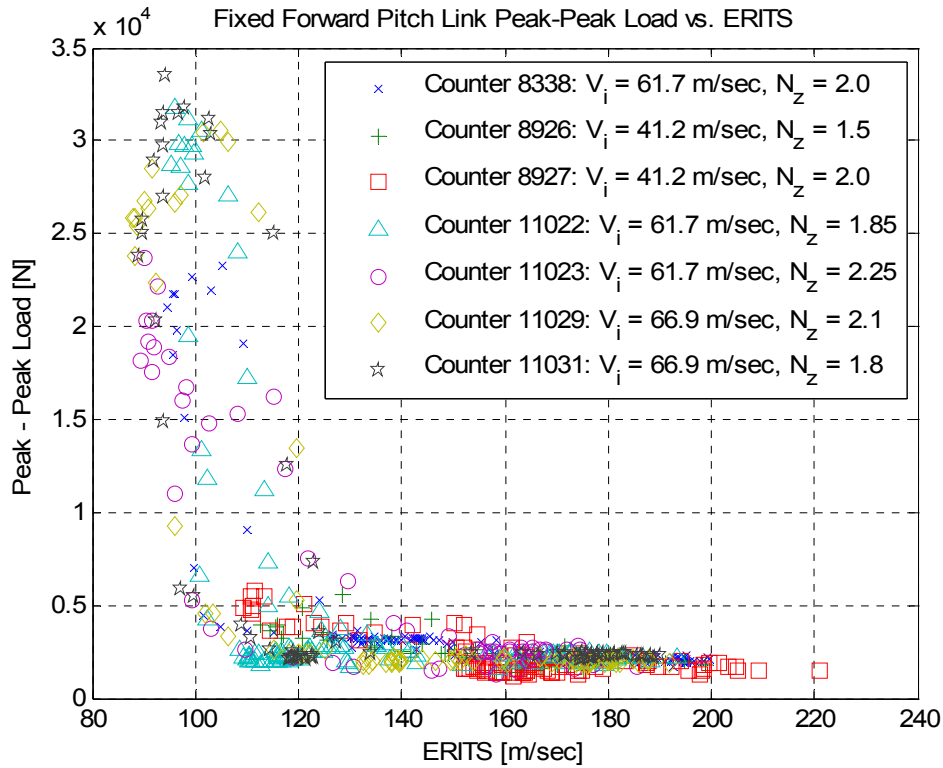


Figure 10: Level Flight Fixed Forward Pitch Link Load Variation with ERITS



**Figure 11: Pull-Up Maneuver Fixed Forward Pitch Link Load Variation with ERITS**

Counters 9017 and 8919 shown in Table 1 have already been introduced as two level flight conditions with significantly different pitch link loads. However, even though their pitch link loads are different, their ERITS values are almost identical as shown in Figure 10. In order to determine the reason behind this inconsistency, sectional pitching moments were computed at various radial locations on the blade so that the blade section stall could be identified. As expected, the counter 9017 shows a significant drop in sectional pitching moments at radial locations ranging from 0.675R to 0.965R, the most significant of which occur near 270° and 345° azimuth angles. These stall regions at 0.865R radial locations are shown in Figure 2 for counter 9017. Counter 8919 however shows no such drop in sectional pitching moments as seen from Figure 12 for 0.865R, indicating that there is no blade stall, even though the ERITS value is low (see Figure 10). Therefore, ERITS would provide a false positive signal indicating stall in this case.

The reason why these two level flight conditions have the same ERITS value can be explained by considering the terms in Equation 2. Since both are level flights, the load factor should be very close to one. Weights are also nearly identical at 75620 N (17000 lbs) which implies that the term under the

square root is nearly identical for both cases. The largest difference between these two counters is in density due to the difference in altitude, and the aircraft velocity. Since the counter 9017 is at higher altitude and the counter 8919 is at higher velocity, the first term in the parenthesis of Equation 2 reduces to same value in both cases. Therefore high aircraft velocity will affect the ERITS value as much as altitude will, even though the altitude seems to have more effect on the pitch link loads.

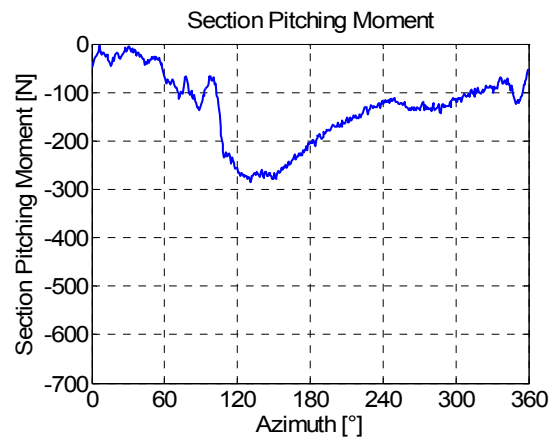


**Figure 12: Sectional Quarter Chord Pitching Moment at 0.865R for Counter 8919**

In the previous section, it is implied that high advance ratio and compressibility effects on the advancing blade will not have significant affect on the increase in pitch link loads as long as weight coefficient is low. That claim is in part confirmed by data from counters 8919 and 9017 shown in Table 1 and Figure 10. Additional data is shown in Figure 13 for further clarification. Also, earlier discussion has pointed out the fact that aircraft velocity will impact the value of ERITS as much as density, while density has greater effect on pitch link loads through the aircraft weight coefficient. Data shown in Figure 13 clarify this point as well.

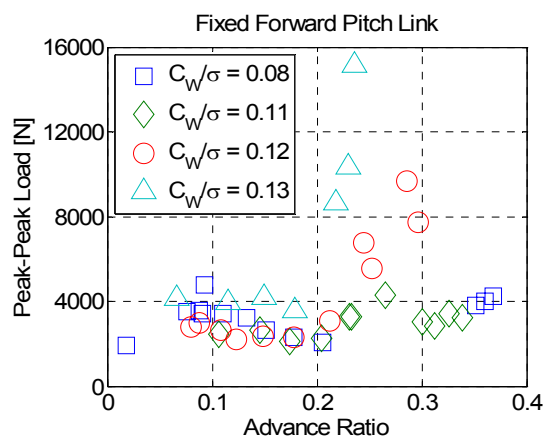


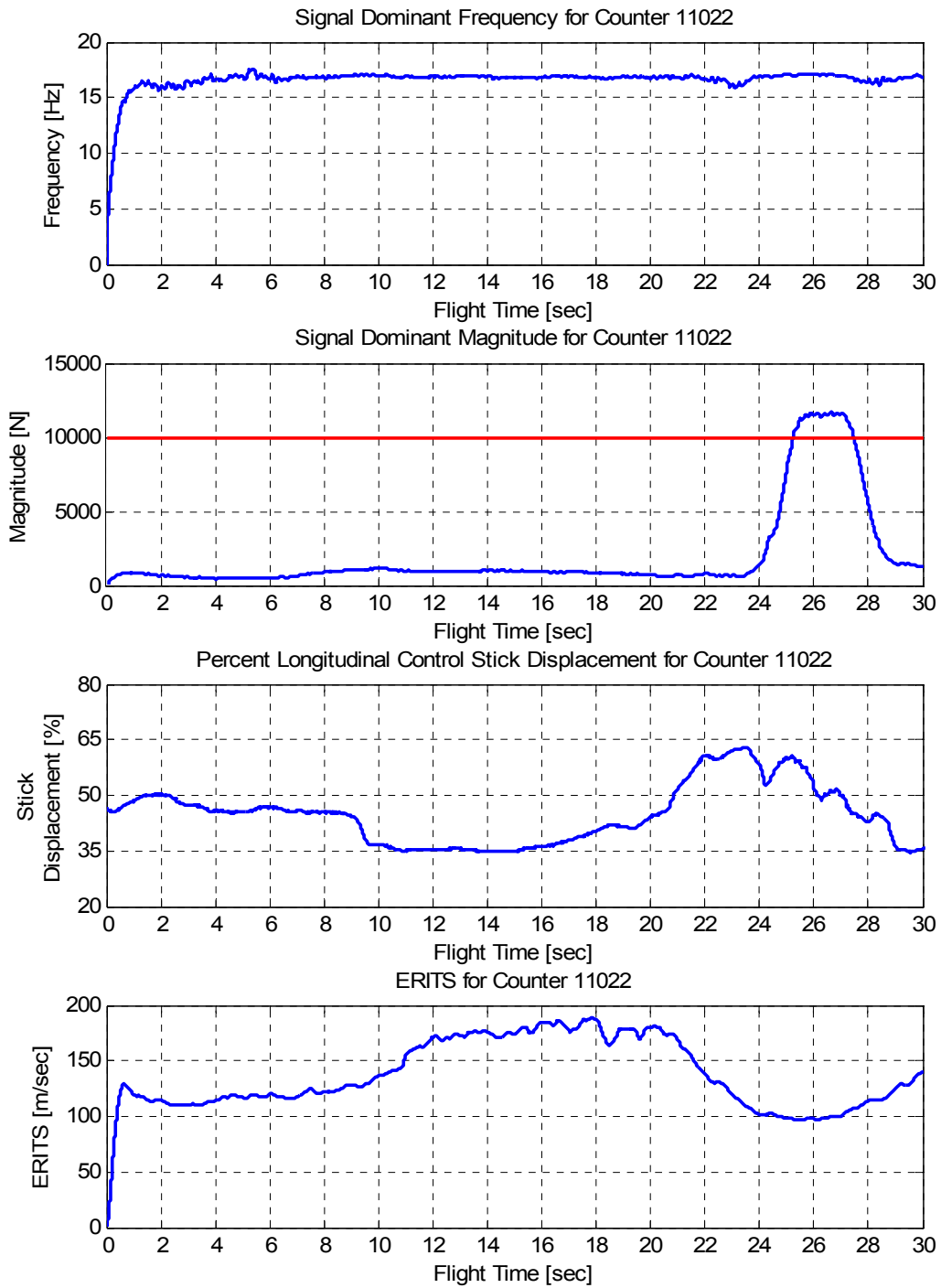
**Figure 13: Fixed Forward Pitch Link Loads vs. Advance Ratio for Level Flights**

### Real-Time Nonlinear Observer (RTNO)

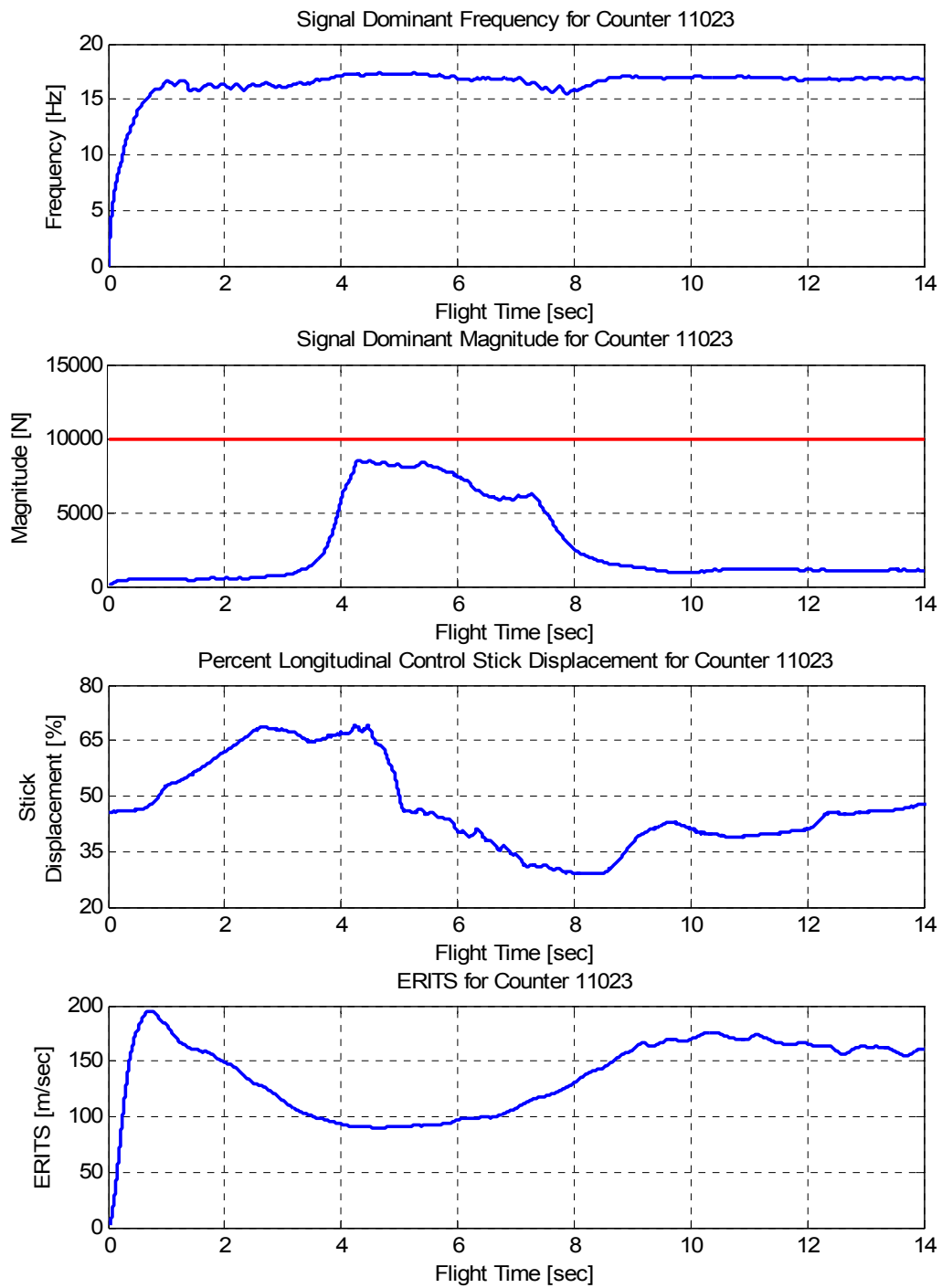
Since one of the major issues of rotor stall is increased pitch link loads, analysis of measured loads on the fixed and rotating pitch links is performed. It was previously observed from spectral analysis of the pitch link load data that there was a significant increase in the fixed pitch link load amplitude at 4/rev (~17 Hz) as the aircraft approached rotor stall. There was also an increase in rotating pitch links load magnitude at 1/rev but to a lesser degree. Results of the spectral analysis are previously shown in Figure 5 for rotating pitch link loads, and Figure 6 for fixed pitch link loads only for level flight data, because more consistent load data is available for a good FFT resolution at level flight than at maneuver flight conditions. The trends are however identical with magnitudes being much higher for pull-up maneuvers. Note that the magnitudes shown in Figure 6 are slightly less than one half of those in Figure 10. This is because the magnitudes shown in

Figure 10 are peak-to-peak magnitudes that include all frequencies. Pitch link load dominant amplitude and the corresponding frequency could be isolated with the implementation of the RTNO. RTNO is an algorithm previously developed at the Georgia Institute of Technology which is able to isolate the dominant signal in a measurement and provide its magnitude and frequency, while at the same time adapting to the variation in frequency such as varying rotor RPM in a maneuver. Neumeier et al. [17] give detailed mathematical description of RTNO. Since the fixed pitch link loads show to be more sensitive to rotor stall than the rotating pitch links, and considering that instrumenting the fixed pitch links is simpler than the rotating ones, only fixed pitch link loads are considered here for the RTNO application.

Figure 14 and Figure 15 show the offline application of the RTNO for two different pull-up maneuvers. First plot in both Figures shows the frequency that corresponds to the dominant load amplitude. This frequency is consistently extracted at around 17 Hz, where 17 Hz corresponds to roughly 4/rev. Second plot shows the 4/rev dominant load amplitude. Since the dominant amplitude in this case is at 17 Hz, the range of frequency used is  $0.5 \text{ Hz} < \omega < 20.5 \text{ Hz}$ . It is possible that at some level flight condition the dominant amplitude is at a frequency other than 4/rev. However, that is found to be the case without stall, where the magnitude is low enough that the frequency does not matter. It may be possible for maneuvers that a dominant fixed pitch link load magnitude is at a frequency other than  $N_b/\text{rev}$  even at rotor stall. That could happen during aggressive maneuvers due to unsteady flow effects. In that case RTNO range of frequencies could be modified to account for all possible frequencies. In Figure 14, maneuver begins at about 20<sup>th</sup> second of the recorded flight time and ends at about 29<sup>th</sup> second. Within that range, the load increases abruptly, clearly indicating that a significant portion of the rotor has stalled. Red line shown on the magnitude plot represents a limit which in this case is selected arbitrarily as 10000 N. If that were to be a true limit, then one would conclude that the maneuver recorded in counter 11022 had entered the overly severe flight regime, not recommended for nominal operation. At the same time, even though the data for counter 11023 indicate that the rotor has entered stall, the severity of that stall is not significant enough based on the set limit.



**Figure 14: Results of the Offline Application of the RTNO for Counter 11022**



**Figure 15: Results of the Offline Application of the RTNO for Counter 11023**

The values of ERITS and the pilot's stick input are also shown in Figure 14 and Figure 15 in order to see the starting points of the pull-up maneuvers. There is a delay of roughly 2 sec from the time the maximum stick input, to the time of corresponding maximum 4/rev pitch link load magnitude estimate, from the RTNO as seen in Figure 14 and Figure 15. An interesting observation is that the counter 11023 (Figure 15) describes the more aggressive maneuver than counter 11022 (Figure 14). Both counters were recorded during pull-up maneuvers at the same indicated airspeed and weight coefficients but with different load factors, 1.85 for counter 11022 and 2.25 for counter 11023. Nevertheless, the pitch link loads are significantly higher for counter 11022 compared to those for counter 11023 as evident from both the RTNO estimates of the 4/rev load magnitudes shown in Figure 14 and Figure 15, and the measured peak-to-peak loads shown in Figure 11. The fact that the maneuver represented by counter 11023 is more aggressive is captured by ERITS, since the ERITS value in the region where maneuver takes place is slightly lower for counter 11023 than for counter 11022. However, the objective is to predict rotor stall as it pertains to pitch link loads and not severity of the maneuver. Therefore ERITS would indicate that the severity of stall was greater for counter 11023 even though the pitch link loads for counter 11023 were lower. Note that the RTNO results shown in Figure 14 and Figure 15 are valid only after about first one second, because RTNO needs that time for initialization. That, however, will not be an issue since, if implemented in real time on the aircraft, RTNO will take that time for initialization while the aircraft is still on the ground.

### Concluding Remarks

Results shown in this paper indicate that the current method of using the Equivalent Retreating Indicated Tip Speed (ERITS) for rotor stall detection is overly conservative. A new, more robust method needs to be developed if one is to design a system that will expand the aircraft flight envelope, and prevent the aircraft from flying in a flight regime that creates significant control loads. A proposed solution to this problem is to instrument the fixed pitch links and to extract the dominant loads and their frequencies with the Real Time Nonlinear Observer (RTNO) algorithm. The limits on the loads extracted by RTNO may be set based on multitude of requirements, including vibration levels and pitch link fatigue properties. Considering that the RTNO method requires the instrumentation of the fixed pitch link loads, an ability to predict rotor stall by estimating the pitch link load magnitude from the

data already available on the aircraft would be a more attractive solution to this problem. Future work will focus on this goal by studying the physics behind the rotor blade dynamics and aerodynamics that contribute to the increase in pitch link loads near stall, as well as blade interaction with the pitch links through the swash plate components.

### Acknowledgments

This project was funded by the U. S. Army under the Vertical Lift Research Center of Excellence (VLRCOE) program managed by the National Rotorcraft Technology Center, Aviation and Missile Research, Development and Engineering Center under Cooperative Agreement W911W6-06-2-0004 between Georgia Institute of Technology and the U. S. Army Aviation Applied Technology Directorate. Dr. Michael Rutkowski is the technical monitor. The authors would like to acknowledge that this research and development was accomplished with the support and guidance of the NRTC. The views and conclusions contained in this document are those of the authors and should not be interpreted as representing the official policies, either expressed or implied, of the Aviation and Missile Research, Development and Engineering Center or the U.S. Government. The authors would also like to acknowledge Mr. Robert M. Kufeld at NASA Ames Research Center for all the assistance related to the UH-60 Airloads Project and TRENDS database.

### References

1. Engineering Design Handbook - Helicopter Engineering - Part One - Preliminary Design, U. S. Army Material Command, Alexandria, VA, 1974.
2. McCroskey, W. J., "The Phenomenon of Dynamic Stall," NASA TM-81264, March 1981.
3. Young, W. H. Jr., "Fluid Mechanics Mechanisms in the Stall Process for Helicopters," NASA TM-81956, March 1981.
4. Datta, A., and Chopra, I., "Prediction of UH-60A Dynamic Stall Loads in High Altitude Level Flight Using CFD/CSD Coupling," *Proceedings of the 61<sup>st</sup> Annual Forum*, American Helicopter Society, Grapevine, TX, June 2005, pp. 117 – 136.
5. Nguyen, K., "Active Control of Helicopter Blade Stall," *Journal of Aircraft*, Vol. 35, No. 1, 1998, pp. 91 – 98.

6. Lorber, P., McCormick, D., Anderson, T., Wake, B., MacMartin, D., Pollack, M., Corke, T., and Breuer, K., "Rotorcraft Retreating Blade Stall Control," AIAA Paper 2000-2475, June 2000.

7. Voskuijl, M., Walker, D. J., Manimala, B., and Kureemun, R., "First Steps Toward the Design of an Active Pitch Link Loads Reduction System Using Novel Control Technologies," *Proceedings of the 31<sup>st</sup> European Rotorcraft Forum*, Florence, Italy, Sep. 2005.

8. Kottapalli, S., "A More Accurate Characterization of UH-60A Pitch Link Loads Using Neural Networks," NASA Ames Research Center, Nov. 1998.

9. Jeram, G. J., "Open Design for Helicopter Active Control Systems," *Proceedings of the 58<sup>th</sup> Annual Forum*, American Helicopter Society, Montreal, Canada, June 2002, pp. 2435 – 2454.

10. Yavrucuk, I., Unnikrishnan, S., and Prasad, J. V. R., "Envelope Protection in Autonomous Unmanned Aerial Vehicles," *Proceedings of the 59<sup>th</sup> Annual Forum*, American Helicopter Society, Phoenix, AZ, May 2003, pp. 2000 – 2010.

11. Bondi, M. J. and Bjorkman, W. S., "TRENDS – A Flight Test Relational Database, User's Guide and Reference Manual," NASA TM-108806, June 1994.

12. Kufeld, R. M., Balough, D. L., Cross, J. L., Studebaker, K. F., Jennison, C. D. and Bousman, W. G., "Flight Testing the UH-60A Airloads Aircraft," *Proceedings of the 50<sup>th</sup> Annual Forum*, American Helicopter Society, Washington D. C., May 1994, pp. 557 – 578.

13. Coleman, C. P. and Bousman, W. G., "Aerodynamic Limitations of the UH-60A Rotor," NASA TM-110396, Aug. 1996.

14. Bousman, W. G., "Characterization of Dynamic Stall on the UH-60A," NASA TM-98-112240, 1998, pp. 32.

15. Kufeld, R. M., and Johnson, W., "The Effects of Control System Stiffness Models of the Dynamic Stall Behavior of a Helicopter," *Proceedings of the 54<sup>th</sup> Annual Forum*, American Helicopter Society, Washington, D.C., May 1998, pp. 589 – 601.

16. Kufeld, R. M., and Bousman, W. G., "High Load Conditions Measured on a UH-60A in Maneuvering Flight," *Proceedings of the 51<sup>st</sup> Annual Forum*,

American Helicopter Society, Fort Worth, TX, May 1995, pp. 421 – 433.

17. Neumeier, Y., Markopoulos, N. and Zinn, B. T., "A Procedure for Real-Time Mode Decomposition, Observation, and Prediction for Active Control of Combustion Instabilities," *Proceedings of the 1997 International Conference on Control Applications*, Institute of Electrical and Electronics Engineers, Hartford, CT, Oct. 1997, pp. 818 – 823.

## Appendix

### Derivation of ERITS Expression

Consider the lift of the individual blade to be expressed as shown in Equation 3.

$$L = \frac{1}{2} C_L \rho V_{rel}^2 S \quad (3)$$

Since the assumption is that rotor stall is directly related to the retreating blade stall, we will assume that  $V_{rel} = \Omega R - V$ . This is clearly not true for the entire blade, but we are only considering the blade tip with a simplifying assumption of uniform lift distribution along the blade. The purpose here is not to calculate the lift distribution on the retreating blade but merely to develop parameter that will vary appropriately as the rotor approaches stall. . Since we are considering the worst case condition, let us also consider the case where the retreating blade lift (L) is roughly the rotor thrust (T) divided by the number of blades ( $N_b$ ) i.e.  $T = N_b L$ . Then we can write the following.

$$T = \sqrt{(N_z W)^2 + D^2} \quad (4)$$

$$\frac{N_b}{2} C_L \rho V_{rel}^2 S = \sqrt{(N_z W)^2 + D^2} \quad (5)$$

$$\frac{N_b}{2} C_L S = \frac{\sqrt{(N_z W)^2 + D^2}}{\rho(\Omega R - V)^2} \quad (6)$$

$$\sqrt{\frac{2}{N_b C_L S}} = \frac{\sqrt{\rho(\Omega R - V)}}{\sqrt[4]{(N_z W)^2 + D^2}} \quad (7)$$

Multiplying by  $\sqrt{W_0/\rho_{SL}}$  and considering that the

indicated velocity is defined as  $V_i = V\sqrt{\rho/\rho_{SL}}$ , we

get the following equality where the right hand side is the expression for ERITS.

$$\sqrt{\frac{2W_0}{N_b\rho_{SL}C_L S}} = \left( \Omega R \sqrt{\frac{\rho}{\rho_{SL}}} - V_i \right) \sqrt{\frac{W_0^2}{(N_z W)^2 + D^2}}$$

Considering that the effect of drag is negligible, we can set  $D = 0$  such that the final expression for ERITS reduces into expression as one shown in Equation 2. Since  $W_0$  is an arbitrary value that can be either an empty weight, take off weight or any other value, it should always be specified when ERITS values are presented. In this paper  $W_0$  value was chosen as 73396 N (16,500 lbs).

$$ERITS = \left( \Omega R \sqrt{\frac{\rho}{\rho_{SL}}} - V_i \right) \sqrt{\frac{W_0}{N_z W}} \quad (2')$$

Since  $W_0$ ,  $N_b$ ,  $\rho_{SL}$ , and  $S$  are all constant, we can see that the ERITS in some effect is inversely proportional to the square root of the retreating blade lift coefficient. Therefore, when the retreating blade lift coefficient is high, the blade should stall and that should be evident in the low values of ERITS. Unfortunately, ERITS also indicates rotor stall in cases where rotor stall did not occur, making it an overly conservative rotor stall detection method.